Polycomb-Mediated Chromatin Loops Revealed by a Sub-Kilobase Resolution Chromatin Interaction Map

Kyle P. Eagen[a,1,2], Erez Lieberman Aiden[b,c,d,e], Roger D. Kornberg[a,2]

[a]Department of Structural Biology, Stanford University School of Medicine, Stanford, CA 94305, USA

[b]The Center for Genome Architecture, Baylor College of Medicine, Houston, TX 77030, USA

[c]Department of Molecular and Human Genetics, Baylor College of Medicine, Houston, TX 77030, USA

[d]Center for Theoretical Biological Physics, Rice University, Houston, TX 77005, USA

[e]Department of Computer Science, Rice University, Houston, TX 77005, USA

[1]Present address: Department of Biochemistry and Molecular Genetics, Northwestern University Feinberg School of Medicine, Chicago, IL 60611, USA

[2]To whom correspondence should be addressed. Email: eagen@northwestern.edu and kornberg@stanford.edu

Classification: BIOLOGICAL SCIENCES: Biochemistry

Keywords**:** DNA loops, Polycomb, gene repression, CTCF, Hi-C, chromosome structure, nuclear architecture, *Drosophila melanogaster*

The authors declare no conflict of interest.

Data deposition: The Hi-C sequence data reported in this paper have been deposited at the GEO database, www.ncbi.nlm.nih.gov/geo (accession no. GSE89112).

ABSTRACT

The locations of chromatin loops in *Drosophila* were determined by Hi-C (chemical cross-linking, restriction digestion, ligation, and high-throughput DNA sequencing). Whereas most loop boundaries or “anchors” are associated with CTCF protein in mammals, loop anchors in *Drosophila* were found most often in association with the polycomb group (PcG) protein Polycomb (Pc), a subunit of Polycomb Repressive Complex 1 (PRC1). Loops were frequently located within domains of PcG-repressed chromatin. Promoters located at PRC1 loop anchors regulate some of the most important developmental genes and are less likely to be expressed than those not at PRC1 loop anchors. Although DNA looping has most commonly been associated with enhancer-promoter communication, our results indicate that loops are also associated with gene repression.

INTRODUCTION

Active and inactive genes are folded differently and located in different regions of the nucleus, but the molecular basis of chromosome folding and nuclear architecture remains to be determined. One folding paradigm is the formation of protein-mediated DNA loops, which are most commonly associated with enhancer-promoter communication (1). On the other hand, gene repression is most often associated with heterochromatin formation and chromosome condensation.

Chromosome folding can be revealed by chemical cross-linking, followed by restriction digestion, ligation, and high-throughput DNA sequencing (2). Such “Hi-C” analysis has revealed intra-chromosomal folding on multiple length scales. From lengths of 1 kb, the smallest so far examined (3), to hundreds of kb, two features are observed, loops (3) and so-called topologically associating domains, or “TADs” (which we and others have also referred to as A/B domains, physical domains, topological domains or contact domains) (3-7). Loops bring a pair of loci into close physical proximity; TADs represent genomic intervals in which all pairs of loci exhibit an enhanced frequency of contact, and correspond to stably condensed chromosomal regions (8). On a larger scale, extending to whole chromosomes, TADs interact with one another to form “compartments” (2).

Hi-C on the smallest length scale, based on the most extensive sequencing, is needed for unambiguous identification of chromatin loops, and has been reported thus far only for the mouse and human genomes (3). We have now overcome this limitation in

Drosophila, by Hi-C analysis at sub-kilobase resolution. We find an unanticipated correlation with results of ChIP-seq analysis in *Drosophila*, with an important functional correlate.

RESULTS

Sub-kilobase resolution *Drosophila* Hi-C

We performed Hi-C on embryonic Kc167 *Drosophila melanogaster* cultured cells and identified 529 million chromosomal contacts (read pairs that remain after exclusion of duplicates, unligated fragments, and reads that align poorly with genome sequences). The resolution of the resulting contact maps was 260 bp, or "sub-kilobase", based on standard metrics (3) (Fig. S1, Table S1, and Methods). For this reason, and because 77.1% of the restriction fragments used for the Hi-C analysis were shorter than 500 bp, we plotted the contact maps in units of at least 500 bp. The contact maps were 3- to 4-fold more dense than those previously reported for human cells at kilobase resolution (3).

Consistent with previously reported *Drosophila* Hi-C contact maps (4, 8, 9), we observed both TADs (apparent in a Hi-C contact map as boxes of enriched contact frequency tiling the diagonal; Fig. 1A and 1B) and compartments (apparent as off-diagonal boxes of alternating enriched or depleted contacts, whose boundaries are aligned with those of the on-diagonal boxes; Fig. 1a,b and Table S2). We identified more TADs in Kc cells than were originally reported (9) (2,126 versus 1,110; Table S2) because more TAD boundaries could be detected at higher resolution (3). We also

identified chromatin loops, which appeared as focal peaks of contact enrichment (Fig. 1C and Table S3), and which were previously unobservable in lower resolution *Drosophila* maps.

Drosophila **Loops Are Unrelated to TADs**

We identified 120 chromatin loops, far fewer than the number of TADs, and also far fewer than the 9,448 loops identified in human GM12878 B-lymphoblastoid cells (3), even after accounting for the difference in genome size.

Drosophila loops differed from mammalian loops in their relationship to TADs (Fig. 1D). Mammalian loop anchors are frequently (38% of loops) located at TAD corners, and therefore coincide with TAD boundaries. In contrast, the vast majority (82.5%) of *Drosophila* loops did not appear at TAD corners (Fig. 1C), and conversely, 99.1% of *Drosophila* TADs did not have focal peaks at their corners. Evidently, chromatin condensation revealed by TADs (8) is not due in *Drosophila* to loops detectable by our methods.

Lack of CTCF at ***Drosophila*** **Loop Anchors**

In humans, 86% of loop anchors are associated with CTCF, and the CTCF-binding motifs are in a convergent orientation (3, 10). In contrast, *Drosophila* loop anchors did not tend to align with CTCF ChIP-seq signals (11) (Fig. 2A and 2B), and only 28.2% of loop anchors overlapped CTCF-binding sites genome-wide (Fig. 2C). Loop anchors were less likely to occur at the strongest CTCF ChIP-seq peaks than at the weakest

peaks (Fig. 2C, left). Conversely, the strongest CTCF ChIP-seq peaks were less likely to occur at loop anchors than at the weakest peaks (Fig. 2C, right). At a minimum ChIP enrichment of 16-fold, loop anchors are 9.55-fold enriched at CTCF sites, but this accounts for only 13.2% of loop anchors and 1.66% of CTCF sites. Evidently, CTCF is rarely, if ever, significantly associated with chromatin loops, and the vast majority of CTCF sites are unrelated to the chromatin loops we identify in *Drosophila*. Similar results were obtained for the other *Drosophila* insulator proteins BEAF-32, Su(Hw), and CP190 (Fig. S2). In contrast to the results for CTCF, and in keeping with reports for human loop anchors, the majority (72.8%) of *Drosophila* loop anchors were associated with the cohesin subunit Rad21. Moreover, stronger Rad21 ChIP peaks were more likely to overlap with loop anchors (Fig. 2A, 2B, and 2D).

Loops are Found within Polycomb-Repressed Chromatin

For a more comprehensive assessment of the relationship between loops, loop anchors, and chromatin-bound proteins, we compared our loop annotation to the five functional classes of chromatin that were previously identified on the basis of genome-wide non-histone protein localization in *Drosophila* Kc cells: PcG-repressed chromatin, HP1 heterochromatin, another type of repressed chromatin ("null/inactive"), and two types of active chromatin ("H3K36me3-enriched or –depleted") (12). We found that 17.5% of loops were entirely contained within a region of PcG-repressed chromatin, and such enrichment of entire loops within PcG-repressed chromatin was far greater than expected on a random basis (10.9-fold, $P = 1.82 \times 10^{-35}$) (Fig. 2E). Few loops were entirely located within H3K36me3-enriched or -depleted active chromatin (no loops), or

HP1 heterochromatin (0.8% of loops), and loops were neither significantly enriched nor depleted from these classes (Fig. 2E). Loops were depleted from null/inactive chromatin (2.5% of loops, a 5.1-fold depletion, $P = 5.07 \times 10^{-4}$). The low percentage of loops entirely located within a single functional chromatin class indicates that the majority of loops must span more than one class.

Many loop anchors (39.6%) were located within PcG-repressed chromatin, and enrichment of loop anchors within PcG-repressed chromatin was greater than expected on a random basis (2.35-fold, $P = 1.79 \times 10^{-16}$) (Fig. 2E). A smaller fraction of loop anchors was found in H3K36me3-depleted active chromatin (18.8% of anchors, 2.76-fold enriched, $P = 6.01 \times 10^{-10}$) (Fig. 2E). Loop anchors were significantly depleted from HP1 heterochromatin, null/inactive chromatin, and H3K36me3-enriched active chromatin (HP1: 0.1% of anchors, 3.32-fold depletion, $P = 0.0436$; null/inactive: 17.8%, 2.47-fold depletion, $P = 1.19 \times 10^{-14}$; H3K36me3-enriched active: 8.42%, 1.82-fold depletion, $P = 7.07 \times 10^{-3}$) (Fig. 2E).

The Polycomb Protein is Found at Loop Anchors

PcG proteins are involved in gene repression during development and are components of two evolutionarily conserved complexes, PRC1 and PRC2. PRC2 trimethylates histone H3 at lysine 27, which demarcates PcG-repressed chromatin and is bound by the chromodomain of the Polycomb (Pc) subunit of PRC1 (13). Loops were readily identified within H3K27me3-enriched regions (14) (Fig. 2A, 2B, 3A, and 3B), and loop anchors tended to coincide with Pc ChIP-seq signals (15) from Kc cells (Fig. 2A, 2B, 3A,

and 3B). Occasionally, loop anchors that aligned with Pc ChIP signals formed networks of interactions (Fig. 2B). Overall, a remarkable 62.4% of loop anchors were associated with Pc ChIP peaks. The enrichment of loop anchors at Pc ChIP peaks increased with the strength of the Pc ChIP peak, and enrichment of Pc ChIP peaks at loop anchors continually increased with the strength of the Pc ChIP peak as well (Fig. 2F). The percentage of Pc ChIP peaks at loop anchors increased 18.8-fold from 2.1% to 39.5% as the strength of the Pc peak increased from 0-fold to 100-fold minimum ChIP enrichment. This is in contrast with CTCF, BEAF-32, Su(Hw), and CP190, none of which exhibited a monotonic relationship between peak strength and the frequency of overlap with loop anchors (Fig. 2C and S2). To ensure that these results reflected the presence of Pc, rather than off-target binding by the antibody that was employed for ChIP, we analyzed ChIP-seq data from a second antibody against Pc (15) and obtained essentially the same results (Fig. S3).

The presence of strong Pc ChIP sites that are not associated with loop anchors may reflect the presence of chromatin loops that we cannot detect. Especially in the case of strong Pc ChIP sites separated by only a few kilobases, it is difficult to identify focal peaks in the Hi-C map due to the strong signal along the diagonal.

PRC1 Loops Are Associated with Gene Repression

We found that Pc ChIP sites enriched at least 30-fold were not only particularly large (in terms of 1D extent along the DNA sequence, see for instance Pc ChIP track in Fig. 2A and 2B), but the majority of these sites (64.2% versus 21.8% for random shuffle control)

contained both GAGA and PHO motifs, which are characteristic of polycomb response elements bound by PRC1 (16). We therefore refer to the anchors found at such sites as "PRC1 loop anchors". Loop anchors were 11.5-fold enriched relative to random shuffle control at these sites, which accounted for 26% of all loop anchors and 26.2% of Pc sites.

A large fraction (32.7%) of PRC1 loop anchors were found at promoters of important developmentally regulated genes, including those for the homeotic PcG target genes *Antennapedia* (*Antp*) and *Sex combs reduced* (*Scr*) at the Antennapedia Hox gene complex (ANT-C) (Fig. 3A), as well as *invected* (*inv*) and *engrailed* (*en*) (Fig. 3B). Gene ontology (GO) term analysis indicated that genes involved in regulating transcription and development were particularly enriched at PRC1 loop-anchor promoters (Fig. 3C and Table S4).

PRC1 loop-anchor promoters were less likely to be expressed than promoters at loop anchors not bound by PRC1 (0 compared to 3 median RPKM expression level, $P = 8.32 \times 10^{-4}$; one-sided Mann–Whitney *U*-test) or promoters not bound by PRC1 and not at loop anchors (0 compared to 3 median RPKM expression level, $P = 1.03 \times 10^{-3}$; one-sided Mann–Whitney *U*-test) (Fig. 3D). Maximum expression levels of promoters at PRC1 loop anchors were less than that of promoters bound by PRC1 but not at loop anchors, even though median expression levels did not significantly differ. A similar result was obtained for promoters at loop anchors not bound by PRC1 compared to promoters not at loop anchors and not bound by PRC1 (Fig. 3D). Taken together, these

197 results suggest a strong relationship between gene repression and chromatin looping,
198 but whether loops cause gene repression or form as a consequence of gene inactivity
199 remains to be determined.
200
201 **DISCUSSION**
202 The locations of loop anchors in *Drosophila* determined here are notable both for
203 correlations with ChIP-seq data and for the lack thereof. The lack of correlation with
204 locations of CTCF protein was unexpected, inasmuch as most loop anchors in
205 mammals are associated with CTCF protein, apparently bound to CTCF sequence
206 motifs in a convergent orientation (3, 10). There are evidently multiple patterns of
207 protein association with loop anchors in metazoans. The association of loop anchors in
208 *Drosophila* with Pc protein is noteworthy because it points to a role of looping not only in
209 gene activation, as widely observed in the past, but in gene repression as well.
210
211 Regions of PcG-repressed chromatin ("PcG domains") that are separated by hundreds
212 of kilobases to megabases are known to be in enhanced spatial proximity (4, 17, 18),
213 but details of their internal organization have only been investigated by averaging over
214 many PcG domains (16). The high resolution of our Hi-C contact maps revealed
215 chromatin loops within individual PcG domains, giving insight into their internal
216 organization. PRC1 is known to compact nucleosome arrays *in vitro* (19). Knockdown
217 of the PRC1 subunit Polyhomeotic (Ph) *in vivo* decompacts PcG-repressed chromatin
218 (20), and Ph that is unable to polymerize impairs the ability of PRC1 to form clusters

(21). Together with these findings, our results suggest that PRC1-bound chromatin loops within PcG-repressed domains either establish or maintain a condensed state.

Previous analyses by 3C have pointed to associations of PcG proteins with chromatin loops for the Bithorax complex (BX-C) in S2 cells (22), for *inv* and *en* in BG3 and Sg4 cells (23), and for an embryonic, pupae, and adult transgenic reporter system (24). Our Hi-C data are, however, at higher resolution and genome-wide. Higher resolution allowed more comprehensive analysis, such as the unambiguous identification of loops and the segmentation of ANT-C into a series of TADs with one or two homeotic gene promoters per TAD (Fig. S4). Genome-wide analysis revealed both the pervasive nature of Pc protein association and the absence of significant CTCF protein association, despite conservation of CTCF from *Drosophila* to human (25).

Another report on *Drosophila* chromatin loops in Kc167 cells appeared while our manuscript was in preparation (26). The other authors noted an enrichment of cohesin but a lack of *Drosophila* CTCF at loop anchors, consistent with our observations. The other authors did not mention Polycomb, but our analysis of their data revealed an enrichment of loop anchors at Pc ChIP peaks and an enrichment of Pc ChIP peaks at loop anchors (Fig. S5). We find a likelihood of repression of promoters at Pc-bound loop anchors, especially for developmental genes; the other authors observed an enrichment of active developmental enhancers at loop anchors, possibly because these are among the many loop anchors not bound by Pc, or because the chromatin at these

241 loop anchors is bivalent, bound by non-histone proteins and histone post-translational
242 modifications associated with both gene activation and repression (27).
243
244 The occurrence of PRC1 at loop anchors could reflect a role in loop formation similar to
245 that proposed for CTCF in mammals, wherein cohesin-complexes extrude loops, in a
246 process halted upon reaching bound CTCF (10, 28, 29). Consistent with this model, a
247 large majority (72.8%) of Drosophila loop anchors are bound by the Rad21 subunit of
248 cohesin. Regardless of whether PRC1 performs such a role, additional proteins must
249 be involved, because PRC1 is present at only 26% of *Drosophila* loop anchors.
250

MATERIALS AND METHODS

Hi-C

Hi-C was performed using the tethered conformation capture approach (8, 30), which improves the signal-to-noise ratio needed for detection of chromatin loops. In brief, *Drosophila melanogaster* Kc167 cultured cells were fixed with 1% EM grade paraformaldehyde. Cells were lysed and cross-linked proteins were biotinylated at cysteine residues and the DNA digested with DpnII. Digested chromatin was bound to streptavidin beads, thoroughly washed to remove uncross-linked DNA, DNA ends filled in with biotin-14-dATP, and free DNA ends ligated together. DNA-protein cross-links were reversed, DNA purified, biotinylated nucleotides marking unligated ends removed, and the DNA sheared to approximately 500 bp. The biotinylated DNA was pulled down with streptavidin beads, prepared for and subjected to high-throughput Illumina DNA sequencing. Further details provided in *SI Appendix, Supplementary Materials and Methods*.

Hi-C Analysis

Hi-C data was analyzed using the Juicer pipeline as previously described (3, 31). In brief, Hi-C reads were mapped to the dm3 reference genome using BWA-MEM. Aligned reads were assigned to restriction fragments, duplicates removed, reads with a MAPQ < 30 removed, and intra-fragment reads removed. The genome was then divided into equally spaced bins and the number of contacts was counted in each pair of bins. Hi-C contact maps were normalized by matrix balancing (3, 31).

TADs were identified using the previously described Arrowhead algorithm (3, 31) and loops were identified by visual inspection and manual annotation using Juicebox (32). Further details provided in *SI Appendix, Supplementary Materials and Methods*.

External datasets used in this study can be found in Table S5.

AUTHOR CONTRIBUTIONS

K.P.E. conceived the project, designed the study, performed Hi-C experiments, and analyzed the data. All authors discussed and interpreted the results. K.P.E. and R.D.K. wrote the manuscript with comments from E.L.A.

ACKNOWLEDGEMENTS

We are grateful to Suhas S.P. Rao for suggestions regarding loop annotation and Su-Chen Huang and Olga Dudchenko for assistance with DNA sequencing. This research was supported by NIH grants GM36659 and AI21144 to R.D.K. and by NIH New Innovator Award 1DP2OD008540, NIH 4D Nucleome Grant U01HL130010, NSF Physics Frontier Center PHY-1427654, Welch Foundation Q-1866, Cancer Prevention Research Institute of Texas Scholar Award R1304, an NVIDIA Research Center Award, an IBM University Challenge Award, a Google Research Award, a McNair Medical Institute Scholar Award, and the President's Early Career Award in Science and Engineering to E.L.A.

REFERENCES

1. Schleif R (1992) DNA looping. *Annu Rev Biochem* 61(1):199–223.

2. Lieberman-Aiden E, et al. (2009) Comprehensive Mapping of Long-Range Interactions Reveals Folding Principles of the Human Genome. *Science* 326(5950):289–293.

3. Rao SSP, et al. (2014) A 3D map of the human genome at kilobase resolution reveals principles of chromatin looping. *Cell* 159(7):1665–1680.

4. Sexton T, et al. (2012) Three-dimensional folding and functional organization principles of the Drosophila genome. *Cell* 148(3):458–472.

5. Nora EP, et al. (2012) Spatial partitioning of the regulatory landscape of the X-inactivation centre. *Nature* 485(7398):381–385.

6. Dixon JR, et al. (2012) Topological domains in mammalian genomes identified by analysis of chromatin interactions. *Nature* 485(7398):376–380.

7. Zhang Y, et al. (2012) Spatial organization of the mouse genome and its role in recurrent chromosomal translocations. *Cell* 148(5):908–921.

8. Eagen KP, Hartl TA, Kornberg RD (2015) Stable Chromosome Condensation Revealed by Chromosome Conformation Capture. *Cell* 163(4):934–946.

9. Hou C, Li L, Qin ZS, Corces VG (2012) Gene density, transcription, and insulators contribute to the partition of the Drosophila genome into physical domains. *Mol Cell* 48(3):471–484.

316 10. Sanborn AL, et al. (2015) Chromatin extrusion explains key features of loop and
317 domain formation in wild-type and engineered genomes. *Proceedings of the*
318 *National Academy of Sciences* 112(47):E6456–65.

319 11. Wood AM, et al. (2011) Regulation of chromatin organization and inducible gene
320 expression by a Drosophila insulator. *Mol Cell* 44(1):29–38.

321 12. Filion GJ, et al. (2010) Systematic protein location mapping reveals five principal
322 chromatin types in Drosophila cells. *Cell* 143(2):212–224.

323 13. Piunti A, Shilatifard A (2016) Epigenetic balance of gene expression by Polycomb
324 and COMPASS families. *Science* 352(6290):aad9780–aad9780.

325 14. Van Bortle K, et al. (2012) Drosophila CTCF tandemly aligns with other insulator
326 proteins at the borders of H3K27me3 domains. *Genome Res* 22(11):2176–2187.

327 15. Li L, et al. (2015) Widespread Rearrangement of 3D Chromatin Organization
328 Underlies Polycomb-Mediated Stress-Induced Silencing. *Mol Cell* 58(2):216–231.

329 16. Schuettengruber B, et al. (2014) Cooperativity, specificity, and evolutionary
330 stability of Polycomb targeting in Drosophila. *Cell Reports* 9(1):219–233.

331 17. Tolhuis B, et al. (2011) Interactions among Polycomb domains are guided by
332 chromosome architecture. *PLoS Genet* 7(3):e1001343.

333 18. Bantignies F, et al. (2011) Polycomb-dependent regulatory contacts between
334 distant Hox loci in Drosophila. *Cell* 144(2):214–226.

335 19. Francis NJ, Kingston RE, Woodcock CL (2004) Chromatin compaction by a

polycomb group protein complex. *Science* 306(5701):1574–1577.

20. Boettiger AN, et al. (2016) Super-resolution imaging reveals distinct chromatin folding for different epigenetic states. *Nature* 529(7586):418–422.

21. Wani AH, et al. (2016) Chromatin topology is coupled to Polycomb group protein subnuclear organization. *Nat Commun* 7:10291.

22. Lanzuolo C, Roure V, Dekker J, Bantignies F, Orlando V (2007) Polycomb response elements mediate the formation of chromosome higher-order structures in the bithorax complex. *Nat Cell Biol* 9(10):1167–1174.

23. Schaaf CA, et al. (2013) Cohesin and polycomb proteins functionally interact to control transcription at silenced and active genes. *PLoS Genet* 9(6):e1003560.

24. Comet I, Schuettengruber B, Sexton T, Cavalli G (2011) A chromatin insulator driving three-dimensional Polycomb response element (PRE) contacts and Polycomb association with the chromatin fiber. *Proceedings of the National Academy of Sciences* 108(6):2294–2299.

25. Moon H, et al. (2005) CTCF is conserved from Drosophila to humans and confers enhancer blocking of the Fab-8 insulator. *EMBO Rep* 6(2):165–170.

26. Cubeñas-Potts C, et al. (2016) Different enhancer classes in Drosophila bind distinct architectural proteins and mediate unique chromatin interactions and 3D architecture. *Nucleic Acids Res*. doi:10.1093/nar/gkw1114.

27. Bernstein BE, et al. (2006) A bivalent chromatin structure marks key

356 developmental genes in embryonic stem cells. *Cell* 125(2):315–326.

357 28. Fudenberg G, et al. (2016) Formation of Chromosomal Domains by Loop
358 Extrusion. *Cell Reports* 15(9):2038–2049.

359 29. Nasmyth K (2001) Disseminating the genome: joining, resolving, and separating
360 sister chromatids during mitosis and meiosis. *Annu Rev Genet* 35(1):673–745.

361 30. Kalhor R, Tjong H, Jayathilaka N, Alber F, Chen L (2012) Genome architectures
362 revealed by tethered chromosome conformation capture and population-based
363 modeling. *Nat Biotechnol* 30(1):90–98.

364 31. Durand NC, et al. (2016) Juicer Provides a One-Click System for Analyzing Loop-
365 Resolution Hi-C Experiments. *Cell Syst* 3(1):95–98.

366 32. Durand NC, et al. (2016) Juicebox Provides a Visualization System for Hi-C
367 Contact Maps with Unlimited Zoom. *Cell Syst* 3(1):99–101.

368

SI APPENDIX

SUPPLEMENTARY MATERIALS AND METHODS

Cell Culture

Kc167 cells were obtained from the Drosophila Genomics Resource Center (Bloomington, IN). Cells were grown in CCM3 media (HyClone) at 25° C.

Hi-C Library Preparation

Hi-C libraries were prepared using a modification of the previously described tethered conformation capture (TCC) (8, 30) protocol. 1 billion Kc167 cells at a density of 4-6 x 10^6 cells/mL were washed with 20 mL CMM3 media and then cross-linked with 1% EM-grade paraformaldehyde in 450 mL CCM3 media for 10 minutes at room temperature while mixing. Paraformaldehyde was quenched by adding 29.8 mL 2.5 M glycine (150 mM final) and incubating for 5 minutes at room temperature while mixing. Cells were washed with 10 mL ice-cold PBS, pelleted, flash frozen in liquid nitrogen and stored at -80° C.

Cells were thawed, resuspended in 10 mL lysis buffer (10 mM Tris-HCl pH 8.0, 10 mM NaCl, 0.2% Igepal CA-630, 1 mM PMSF, 2 mM bezamidine, 2 µM pepstatin A, 0.6 µM leupeptin), and then incubated on ice for 15 minutes. Cells were transferred to a 15 mL Dounce homogenizer and lysed by applying 15 strokes of pestle B, cooled on ice for 1 minute, followed by applying another 15 strokes of pestle B. The lysate was centrifuged at 2,500 x g for 5 minutes, the pellet washed with 5 mL lysis buffer, centrifuged again at 2,500 x g for 5 minutes, the pellet resuspended in 4.6 mL of wash buffer 1 (50 mM Bis-

392 Tris-HCl pH 6.0, 100 mM NaCl, 10 mM $MgCl_2$, 0.1% SDS), incubated at 65° C for 10
393 minutes, and then immediately cooled on ice.
394
395 1.4 mL 25 mM EZ-link Iodoacetyl-PEG2-Biotin (IPB; in wash buffer 1; Thermo Scientific)
396 was added to the sample and incubated for 1 hour at room temperature while rotating.
397 600 µL of 10% Triton X-100 was added, gently mixed, then 160 µL of 50 U/µL DpnII
398 (NEB) was added and the sample incubated at 37° C for 2 hours while rotating. 1.298
399 mL 10% SDS was added, incubated at 65° C for 30 minutes, and then immediately
400 cooled on ice. The sample was added to a 20 kD MWCO, 3-12 mL Slide-A-Lyzer
401 Dialysis Cassette (Thermo Scientific) and dialyzed at room temperature against 4 L of
402 dialysis buffer (10 mM Tris-HCl pH 8.0, 1 mM EDTA). After 2 hours the buffer was
403 replaced with 4 L of fresh dialysis buffer and dialysis continued overnight.
404
405 800 µL of Dynabeads MyOne Streptavidin T1 beads (Life Technologies) were washed
406 three times with 2 mL PBST (PBS + 0.01% Tween 20) and then resuspended in 1 mL
407 PBST. The dialyzed sample was rapidly added to the beads and incubated at room
408 temperature for 30 minutes while rotating. 50 µL of 25 mM neutralized IPB (treated with
409 10-fold excess β-mercaptoethanol) was added to the sample and then incubated at
410 room temperature for 15 minutes while rotating.
411
412 Beads were washed once with 3 mL PBST, twice with 3 mL wash buffer 2 (10 mM Tris-
413 HCl pH 8.0, 50 mM NaCl, 0.4% Triton X-100), resuspended in 1 mL of wash buffer 2,

414 and divided across 5 equal volume aliquots. 190 µL of a fill-in master mix (654 µL
415 water, 11 µL 1 M $MgCl_2$, 110 µL NEBuffer 2, 7.7 µL 10 mM dTTP, 7.7 µL 10 mM dCTP,
416 7.7 µL 10 mM dGTPαS, 192.5 µL 0.4 mM Biotin-14-dATP, 44 µL 10% Triton X-100) was
417 added to each aliquot followed by 10 µL of 5 U/µL DNA Polymerase I, Large (Klenow)
418 Fragment (NEB) and then incubated at 37° C for 75 minutes while rotating. The
419 reaction was stopped with 10 µL 0.5 M EDTA.
420
421 Each aliquot of beads was washed twice with 500 µL wash buffer 3 (50 mM Tris-HCl pH
422 7.4, 0.4% Triton X-100, 0.1 mM EDTA) and then resuspended in 500 µL of wash buffer
423 3. 8.99 mL of a ligation master mix (37.972 mL water, 5.179 mL 10% Triton X-100,
424 5.179 mL 500 mM Tris-HCl pH 7.5, 100 mM $MgCl_2$, 556 µL 10 mg/mL BSA, 556 µL 100
425 mM ATP, 556 µL 1 M DTT) was added to each aliquot followed by 10 µL 2,000 U/µL T4
426 DNA Ligase (NEB) and then incubated at room temperature for 4 hours while rotating.
427 The reaction was stopped with 400 µL 0.5 M EDTA.
428
429 Beads were collected with a magnet, the supernatant discarded, and the beads
430 resuspended in 300 µL of extraction buffer (50 mM Tris-HCl pH 8.0, 100 mM NaCl, 1
431 mM EDTA, 0.2% SDS). 25 µL 800 U/mL proteinase K (NEB) was added to each aliquot
432 and each aliquot was incubated at 65° C overnight.
433

Beads were collected with a magnet and the supernatant transferred to a fresh tube. The DNA was precipitated with ethanol, washed twice with 70% ethanol, and all aliquots combined and resuspended in a total volume of 75 µL 10 mM Tris-HCl pH 8.0. The sample was incubated at 42° C for 15 minutes followed by addition of 5 µL 1 mg/mL RNase A and incubation at 37° C for 30 minutes. DNA concentration was determined with a Qubit dsDNA HS Assay.

7 µL water, 10 µL 10x NEBuffer 1, 1 µL 10 mg/mL BSA, and 3 µL 100 U/µL exonuclease III was added to 79 µL of DNA (no more than 10 µg DNA per reaction, if more than 10 µg multiple reactions were performed in parallel), and incubated at 37° C for 1 hour. The reaction was stopped by adding 2 µL 0.5 M EDTA, 2 µL 5 M NaCl, and incubating at 70° C for 20 minutes. Total sample volume was adjusted to 130 µL.

DNA was sheared to 500 bp with a Covaris S2 at duty cycle 10%, intensity 4, 200 cycles/burst for 55 seconds. 125 µL of sample was transferred to a fresh tube and the DNA was size-selected by first adding 68.8 µL (0.55x volumes) of SPRIselect beads (Beckman), vortexed to mix, and incubated at room temperature for 5 minutes. Beads were collected with a magnet, the supernatant transfered to a fresh tube. 25 µL of SPRIselect beads were added to the supernatant, vortexed to mix, and incubated at room temperature for 5 minutes. Beads were collected with a magnet, the supernatant discarded, and, while still on the magnet, the beads were washed twice with 200 µL

455 85% ethanol and then air dried. DNA was eluted by resuspending the beads in 53 µL of
456 10 mM Tris-HCl pH 8.0 and incubated at room temperature for 5 minutes. Beads were
457 collected with a magnet, and 51 µL of the eluate was transferred to a fresh tube. DNA
458 concentration was determined with a Qubit dsDNA HS Assay.
459
460 DNA was initially prepared for high-throughput sequencing following the directions for
461 "NEBNext End Prep" and "Adaptor Ligation" in the NEBNext Ultra II DNA Library Prep
462 Kit for Illumina (NEB) (if more than 1 µg of DNA, multiple reactions were performed in
463 parallel). 50 µL of Dynabeads MyOne Streptavidin C1 beads (Life Technologies) were
464 washed twice with 100 µL 1x B&W buffer + 0.05% Tween 20 (2x Bind & Wash (B&W)
465 buffer: 10 mM Tris-HCl pH 7.5, 2 M NaCl, 1 mM EDTA) and then resuspended in 86.5
466 µL of 2x B&W buffer. Adaptor-ligated DNA was added to the beads and incubated at
467 room temperature for 30 minutes while rotating. Beads were collected with a magnet,
468 the supernatant discarded, the beads washed twice with 100 µL 1x B&W buffer + 0.05%
469 Tween 20, and then twice with 100 µL 10 mM Tris-HCl pH 8.0, 1 mM EDTA.
470
471 DNA was eluted by resuspending the beads in 5 µL of 95% freshly deionized
472 formamide, 10 mM EDTA pH 8.0, and incubating at 90° C for 10 minutes. The beads
473 were then cooled to room temperature and collected with a magnet. The supernatant
474 was transferred to a fresh tube and mixed with 15 µL 10 mM Tris-HCl pH 8.0.
475

476 The optimal number of PCR cycles for library amplification was determined by setting
477 up an analytical qPCR reaction: 1 µL water, 1 µL eluted DNA, 1 µL primer mix (2.5 µM
478 NEB Universal PCR Primer, 2.5 µM NEB Index Primer, 2.5 mM $MgCl_2$, 5x SYBR Green
479 I, 5x ROX), 2.5 µL NEBNext Ultra II Q5 Master Mix. The sample was thermocycled on a
480 qPCR machine at 98° C for 30 seconds followed by 25 cycles of 98° C for 10 seconds,
481 65° C for 75 seconds. The linear Rn versus cycle number was plotted to determine the
482 cycle number corresponding to one-third of maximum fluorescence. Final library
483 amplification was performed by setting up the following PCR in duplicate: 10.5 µL water,
484 2.5 µL 10 mM $MgCl_2$, 1 µL 25 µM NEB Universal PCR Primer, 1 µL 25 µM NEB Index
485 Primer, 10 µL eluted DNA, 25 µL NEBNext Ultra II Q5 Master Mix. The sample was
486 thermocycled at 98° C for 30 seconds followed by 3 or 4 cycles (as determined above)
487 of 98° C for 10 seconds, 65° C for 75 seconds, followed by 65° C for 5 minutes, and
488 then held at 4° C. The amplified library was purified as in “Cleanup of PCR
489 Amplification” in the NEBNext Ultra II DNA Library Prep Kit for Illumina (NEB), adjusting
490 the volumes as necessary. The DNA was eluted in 17 µL 10 mM Tris-HCl pH 8.0 and
491 15 µL was collected as the final eluate.
492
493 DNA concentration was determined with a Qubit dsDNA HS Assay, DNA integrity
494 determined by a Bioanalyzer High Sensitivity DNA Chip, and then accurately quantified
495 using a KAPA Library Quantification Kit. DNA was paired-end sequenced on an
496 Illumina NextSeq 500 or HiSeq X instrument.

497

498 **Hi-C Data Processing**

499 Data was processed as previously described (3, 31). In brief, reads were mapped to
500 dm3/BDGP Release 5 of the *Drosophila melanogaster* genome using BWA-MEM, reads
501 were assigned to restriction fragments, duplicates removed, reads with a MAPQ < 30
502 removed, and intra-fragment reads removed. The genome was then divided into
503 equally spaced bins and the number of contacts was counted in each pair of bins.

504

505 We noticed at kilobase and sub-kilobase resolution many empty row/columns of the
506 matrix due to restriction fragments spanning multiple bins. Therefore, for high resolution
507 maps, to account for the uncertainty in the location of the position of the cross-link within
508 each restriction fragment, we randomized the read position within the restriction
509 fragment each read mapped to and then assigned the resulting contact to its respective
510 genomic bin. This improved the quality of the maps as “missing data” was now
511 “recovered” without changing the position of loops or TADs. All subsequent analysis
512 was performed using randomized intrafragment read positions. Based on the previously
513 established metric for Hi-C map resolution (3), the resolution of our Hi-C contact maps
514 is 260 bp. However, this approaches the median restriction fragment length for DpnII
515 (193 bp) and, consequently, may overestimate the true resolution. For the dm3
516 reference genome 77.1% of restriction fragments are shorter than 500 bp, which
517 indicates an appropriate lower bound for map resolution while at the same time
518 recovering high-resolution information from deeply sequenced *Drosophila* Hi-C libraries.

519 Therefore, using the previously defined metric (3), we have attained the maximum
520 possible resolution using DpnII for fragmentation or “sub-kilobase” resolution.
521
522 Hi-C contact maps were normalized by matrix balancing using the KR normalization
523 algorithm (3, 31, 33). All subsequent analysis was performed on KR normalized contact
524 maps. Reproducibility between biological replicates was determined by flattening the
525 Hi-C matrices to vectors and calculating the Pearson’s correlation coefficient (*r*)
526 between the vectors. Biological replicates were highly correlated at all resolutions
527 (Extended Data Fig. 1D). Therefore, datasets were merged after filtering, intrafragment
528 read positions randomized as described above, and the combined contact map KR
529 normalized. All subsequent analysis was performed on the combined, KR normalized
530 contact map.
531
532 TADs were identified using the previously described Arrowhead algorithm (3, 31),
533 except with the addition of a post-processing step. This step was necessary as the
534 Arrowhead algorithm applied at 500 bp resolution skipped some obvious larger
535 domains, whereas the Arrowhead algorithm applied at 5 kb resolution cannot identify
536 smaller domains. Therefore, TADs were identified at 5 kb, 2 kb, 1 kb, and 500 bp
537 resolution using the Arrowhead algorithm, merged into a single list sorted by decreasing
538 corner score, and conflicts, defined as the boundary of one TAD being located within
539 another TAD, resolved by using the greater corner score of any conflicting TADs. Use
540 of the greater corner score ensures that the most prominent, high confidence TADs are
541 identified. Although this procedure precludes the identification of nested TADs, visual

inspection of the resulting TAD annotation revealed excellent agreement with Hi-C contact maps and is consistent with prior annotations of non-nested TADs in *Drosophila* (4, 9).

Drosophila loops were manually annotated by visual identification of focal peaks of contact enrichment using Juicebox (32). The number of Hi-C contacts at peak pixels was enriched relative to four local neighborhoods (donut, bottom left, horizontal, vertical; see reference 3 for full definitions) and this enrichment was significantly greater than the enrichment at a control set of randomly shuffled loops (as described below) thereby validating our manual loop annotation (Fig. S6). For all subsequent analysis, the central 1 kb of each loop anchor was used.

We also used the HiCCUPS algorithm (3, 31) to annotate chromatin loops. HiCCUPS was run with options -k KR -r 1000 -f 0.001 -p 10 -i 20 -t 0.02,2.5,2.5,2.5 -d 20000. We further filtered the loop list by requiring loops to be greater than 10 kb in size (due to the strong signal along the diagonal, it is hard to unambiguously identify very small loops), to result from collapsing more than 3 enriched pixels to a single peak pixel (to eliminate single, double, or triple pixel blowouts from being called a loop), and to be on chromosome X, 2L, 2R, 3L, 3R, or 4. This resulted in 206 loops. Using the manually annotated loop list as a gold standard (3), HiCCUPS had a 75.6% false positive rate and a 57.5% false negative rate. This elevated error rate is likely due to the fact that HiCCUPS was designed to annotate loops in mammals. Visual inspection of the HiCCUPS-annotated loops identified that the majority of false positives were due to the

565 small feature size of *Drosophila* loops and especially TADs, which made HiCCUPS loop
566 annotation difficult at high resolution and resulted in compartment flips being falsely
567 identified as loops. Due to the extremely high false positive rate we only report results
568 using the manual annotation. However, Pc and Rad21 were also significantly enriched
569 at HiCCUPS-annotated loop anchors (Fig. S7) validating conclusions from our manual
570 annotation. As expected for any annotation with many false positives, the enrichment of
571 Pc and Rad21 at HiCCUPS-annotated loop anchors was less than that for manually-
572 annotated loop anchors.
573
574 **Relationships between Loops and TADs**
575 To determine if loops are spatially close to TADs, we determined the Euclidean distance
576 (i.e. the two-dimensional distance between pixels i_1,j_1 and i_2,j_2 in the Hi-C matrix; see
577 reference 8) between a loop (i.e. focal peak of contact enrichment) and the closest TAD
578 corner (smallest Euclidean distance) for all loops. Since TAD sizes differ between flies
579 and humans the Euclidean distance was normalized by the size of the closest TAD for
580 each loop in the respective species.
581
582 To determine if loops overlapped TAD corners, that is if loops demarcate TADs, for
583 every loop at location $M_{i,j}$ we determined if there was a TAD corner within distance
584 0.2*|i-j| of the loop (3). The procedure was repeated for every TAD with TAD corner at
585 $M_{i,j}$ to assess the overlap of TADs with loops.
586
587 **Enrichment of Loop Anchors at Non-histone Protein Binding Sites**

588 ChIP-seq reads were mapped to chromosomes X, 2L, 2R, 3L, 3R, and 4 of the
589 dm3/BDGP Release 5 of the *Drosophila melanogaster* genome using bowtie2 with
590 option --very-sensitive. Reads were filtered to include only properly paired reads and
591 reads with a MAPQ >= 30. PCR duplicates were removed with picard. MACS2 (34)
592 was used to call peaks by running macs2 callpeak with parameters --SPMR --keep-dup
593 -g dm -f BAMPE and signal tracks were computed by running macs2 bdgcmp with
594 parameter -m FE. Histone modification ChIP-seq data was processed as above, except
595 the macs2 callpeak parameters --SPMR --keep-dup all --nomodel --nolambda --broad -g
596 dm -f BAMPE were used.
597
598 The percentage of unique loop anchors at non-histone protein binding sites was
599 calculated by dividing the number of loop anchors overlapping a ChIP-seq peak by the
600 total number of loop anchors.
601
602 For each ChIP-seq dataset we iterated through the list of unique loop anchors counting
603 how many unique loop anchors overlapped with a ChIP-seq peak. We then used
604 bootstrapping to estimate the expected random distribution of counts and to get the
605 significance of enrichment of unique loop anchors at ChIP-seq peaks. This is done by
606 shuffling the order of unique loop anchors while ensuring that anchors remain on their
607 respective chromosome, are not merged in the shuffle, and are excluded from genome
608 assembly gaps. Then, we counted how many shuffled, unique loop anchors overlapped
609 with a ChIP-seq peak. This procedure was repeated 10,000 times generating a new
610 count each time. Enrichments and 95% confidence intervals are then determined by

comparing the observed count of unique loop anchors overlapping ChIP-seq peaks to the distribution of shuffled counts.

Enrichment/Depletion of Loops and Loop Anchors Within Epigenetic Classes

For each epigenetic class as defined in reference 12 we iterated through the list of loops and unique loop anchors counting how many loops/anchors overlapped in their entirety with each epigenetic class. Enrichment/depletion of loops/anchors in each epigenetic class was determined by counting how many unique loops/anchors overlapped in their entirety with an epigenetic class relative to a random shuffle control of loops/anchors using the bootstrapping approach described above, except that a Z-score and p-value for each epigenetic class was used to assess enrichment/depletion by comparing the observed count of unique loops/anchors in each epigenetic class to the distribution of shuffled counts.

The percentage of loops/anchors lying within each epigenetic was calculated by dividing the number of loops/anchors within each epigenetic class by the total number of loops/anchors. Only loops/anchors where the entire loop/anchor overlapped an epigenetic class were considered. Since many loops/anchors overlap two or more epigenetic classes the total percentage of loops/anchors lying within each epigenetic class does not sum to 100%.

PHO and GAGA Motifs at PRC1 Loop Anchors

633 PHO and GAGA motif position weight matrices were based on (35). Motifs were
634 identified using STORM (36) and the percentage of PRC1 loop anchors containing both
635 PHO and GAGA motifs was calculated by dividing the number of PRC1 loop anchors
636 overlapping both a PHO and GAGA motif with the total number of PRC1 loop anchors.
637 10,000 random shuffles of PRC1 loop anchors, similar to that described above, was
638 used as a control. Unique PRC1 loop anchors were identified as those loop anchors
639 overlapping a *Pc* ChIP-seq peak with 30-fold or greater ChIP enrichment.
640
641 **Gene Expression at Loop Anchors**
642 RNA-seq data from modENCODE (37) (modENCODE accession modENCODE_4395)
643 was downloaded from release 5.57 of FlyBase
644 (ftp://ftp.flybase.net/releases/FB2014_03/precomputed_files/genes/gene_rpkm_report_f
645 b_2014_03.tsv.gz). RPKM values were extracted for protein-coding genes (13,931 in
646 total) from the Kc167 cell line dataset (FlyBase ID: FBlc0000269).
647
648 The percentage of unique PRC1 loop anchors at gene promoters (defined as the set of
649 1 kb windows centered on the transcription start site for each gene) was calculated by
650 dividing the number of unique PRC1 loop anchors overlapping a gene promoter by the
651 total number of unique PRC1 loop anchors.
652
653 Significant differences between RNA-seq RPKM values between PRC1 loop-anchor
654 promoters, promoters bound by PRC1 not at loop anchors, promoters at loop anchors

not bound by PRC1, and promoters not at loop anchors and not bound by PRC1 were compared using a one-sided Mann–Whitney *U*-test.

GO term enrichment was performed using DAVID (38) 6.8 Beta (May 2016 knowledgebase) with default parameters. Only GO terms with a Benjamini corrected *P*-value less than or equal to 10^{-3} were considered. REVIGO (39) was used to remove redundant GO terms with default parameters except a cut-off value (*C*) of 0.5 was used and the size of the GO term database was set using the *Drosophila melanogaster* GO annotation database. Reduced redundancy GO term analysis is shown in Fig. 3D, complete GO term analysis is shown in Extended Data Table 3. No cellular component GO terms were significantly enriched.

References

33. Knight PA, Ruiz D (2012) A fast algorithm for matrix balancing. *IMA J Numer Anal* 33(3):drs019–1047.

34. Zhang Y, et al. (2008) Model-based analysis of ChIP-Seq (MACS). *Genome Biol* 9(9):R137.

35. Ringrose L, Rehmsmeier M, Dura J-M, Paro R (2003) Genome-wide prediction of Polycomb/Trithorax response elements in Drosophila melanogaster. *Dev Cell* 5(5):759–771.

36. Schones DE, Smith AD, Zhang MQ (2007) Statistical significance of cis-regulatory modules. *BMC Bioinformatics* 8(1):19.

677 37. Cherbas L, et al. (2011) The transcriptional diversity of 25 Drosophila cell lines.
678 *Genome Res* 21(2):301–314.

679 38. Huang DW, Sherman BT, Lempicki RA (2009) Systematic and integrative analysis
680 of large gene lists using DAVID bioinformatics resources. *Nat Protoc* 4(1):44–57.

681 39. Supek F, Bošnjak M, Škunca N, Šmuc T (2011) REVIGO summarizes and
682 visualizes long lists of gene ontology terms. *PLoS ONE* 6(7):e21800.

683

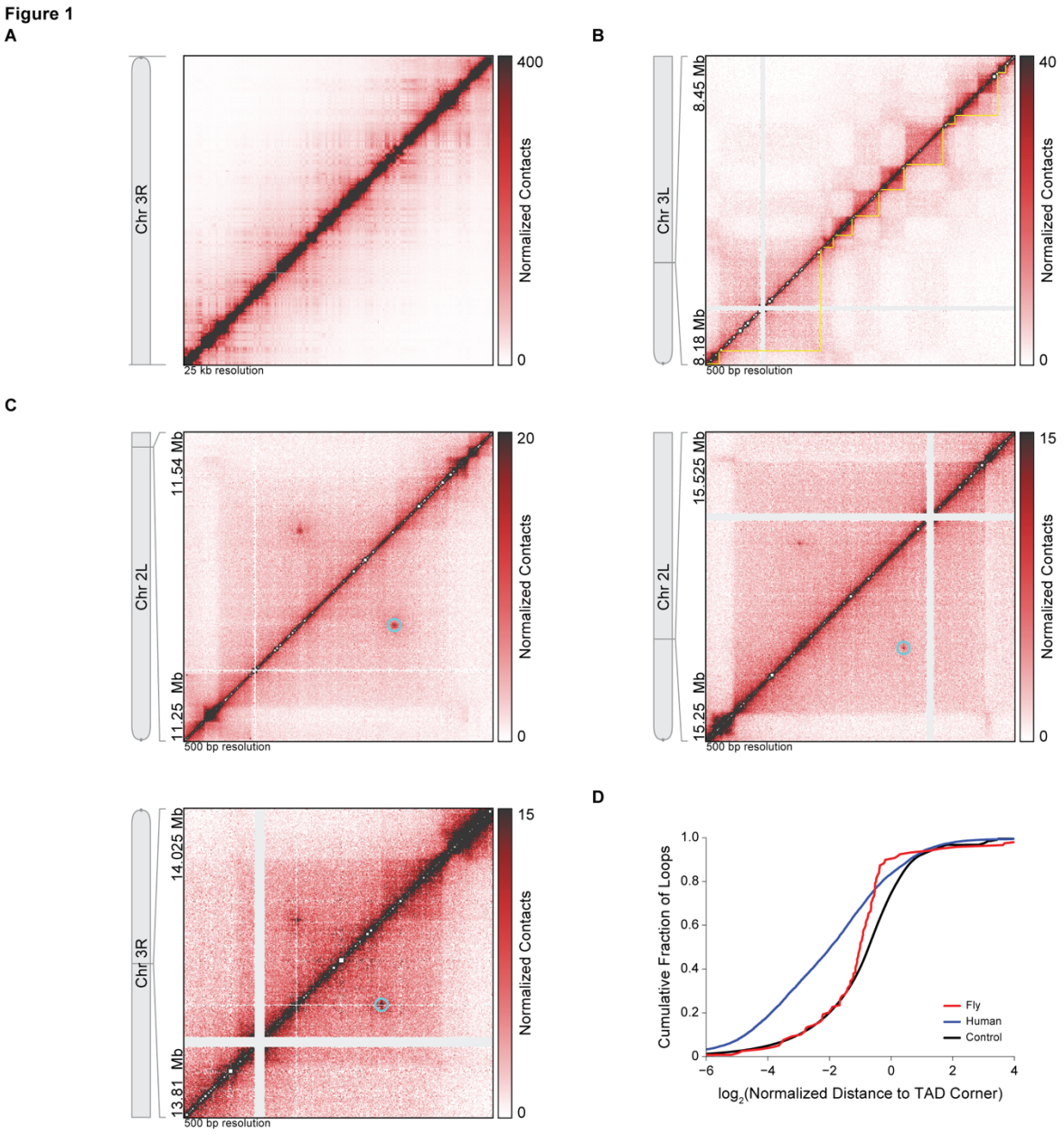

Fig. 1. Sub-kilobase resolution Hi-C identifies *Drosophila* chromatin loops.

(A) Intra-chromosome 3R Hi-C contact map at 25 kb resolution shows off-diagonal boxes of alternating enriched or depleted contacts indicative of compartments.

(B) Hi-C contact map at 500 bp resolution of a region of chromosome 3L shows TADs (yellow outlines) as boxes of enriched contact frequency tiling the diagonal. On-diagonal boxes (TADs) align with off-diagonal boxes indicative of compartmentation.

691 **(C)** Hi-C contact maps at 500 bp resolution reveal the presence of chromatin loops,
692 identified as focal peaks of contact enrichment (cyan circles).
693 **(D)** Cumulative distributions of the two-dimensional Euclidean distance between a loop
694 and the closest TAD corner for *Drosophila* loops (red), human loops (blue), and the
695 mean of 10,000 shuffled sets of *Drosophila* loops (black) with 95% confidence interval
696 (gray shading). *Drosophila* loops are farther from TAD corners than human loops (P =
697 3.79×10^{-11}; two-sided KS test), but closer to TAD corners than the shuffled control (P =
698 5.89×10^{-9}; two-sided KS test). Distance is normalized by TAD size.
699

Figure 2

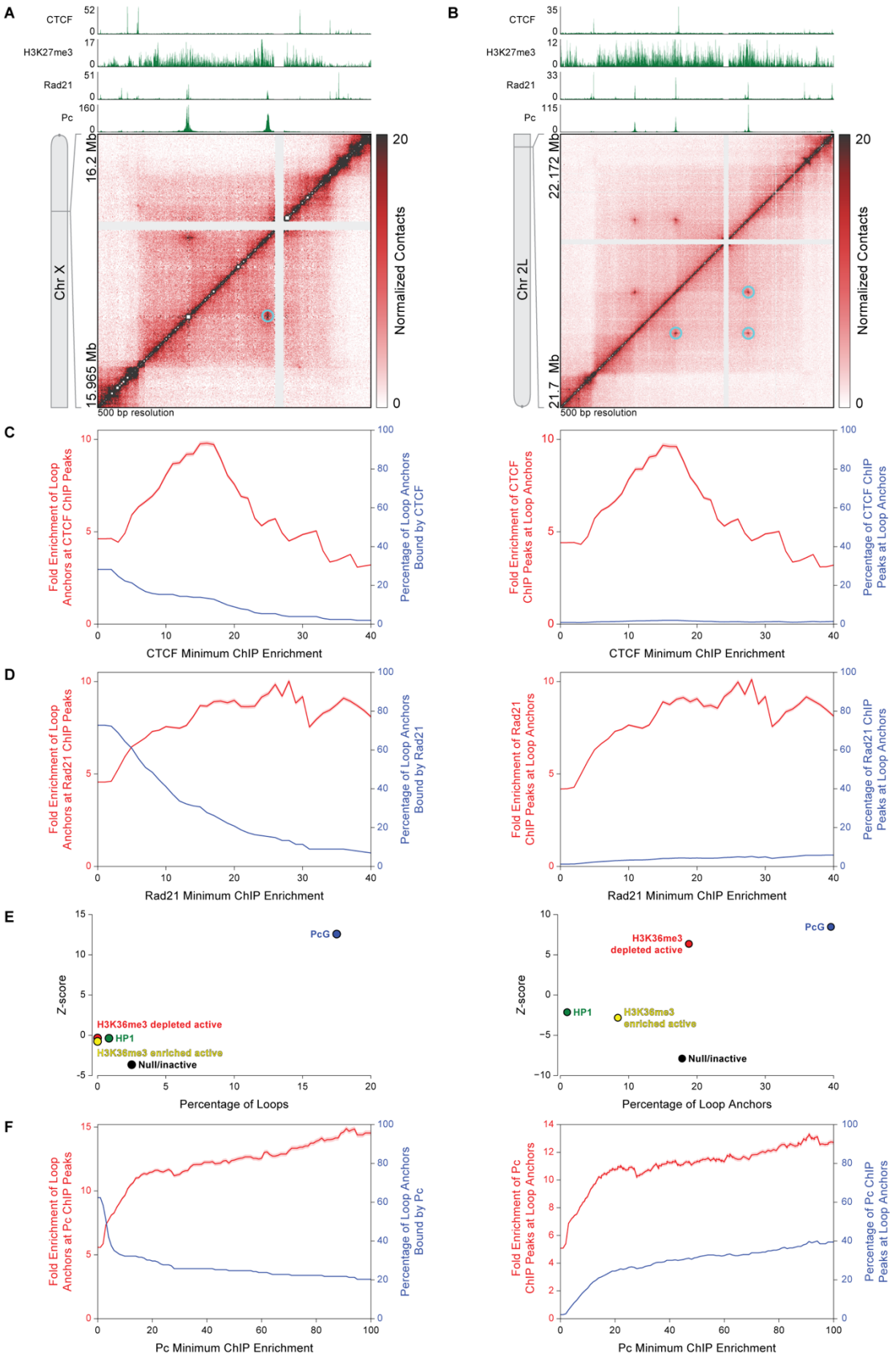

700

Fig. 2. *Drosophila* loop anchors are bound by PRC1.

(A) Hi-C contact map at 500 bp resolution of a region of chromosome X shows chromatin loops (cyan circles) that align with *Pc* ChIP-seq peaks. CTCF, histone H3K27me3, Rad21, and *Pc* ChIP-seq profiles are aligned above the map.

(B) Hi-C contact map at 500 bp resolution of a region of chromosome 2L shows a small network of chromatin loops (cyan circles) that align with *Pc* ChIP-seq peaks. CTCF, histone H3K27me3, Rad21, and *Pc* ChIP-seq profiles are aligned above the map.

(C) Left, fold enrichment of loop anchors at CTCF ChIP peaks (red) and percentage of loop anchors bound by CTCF (blue) at the CTCF minimum ChIP enrichment indicated on the abscissa. Right, fold enrichment of CTCF ChIP peaks at loop anchors (red) and percentage of CTCF ChIP peaks at loop anchors (blue) at the CTCF minimum ChIP enrichment indicated on the abscissa. Red shading indicates 95% confidence interval.

(D) Same as **(C)** except for Rad21.

(E) Left, *Z*-score of the enrichment/depletion of entire loops within five functional classes ("colors") of chromatin relative to 10,000 random shuffle controls shows that entire loops are strongly enriched in PcG-repressed chromatin. Right, *Z*-score of enrichment/depletion of entire loop anchors within five functional classes ("colors") of chromatin relative to 10,000 random shuffle controls shows that entire loop anchors are strongly enriched in PcG-repressed chromatin. Enrichment is given by a positive *Z*-score, depletion by a negative *Z*-score.

(F) Same as **(C)** except for *Pc*.

Figure 3

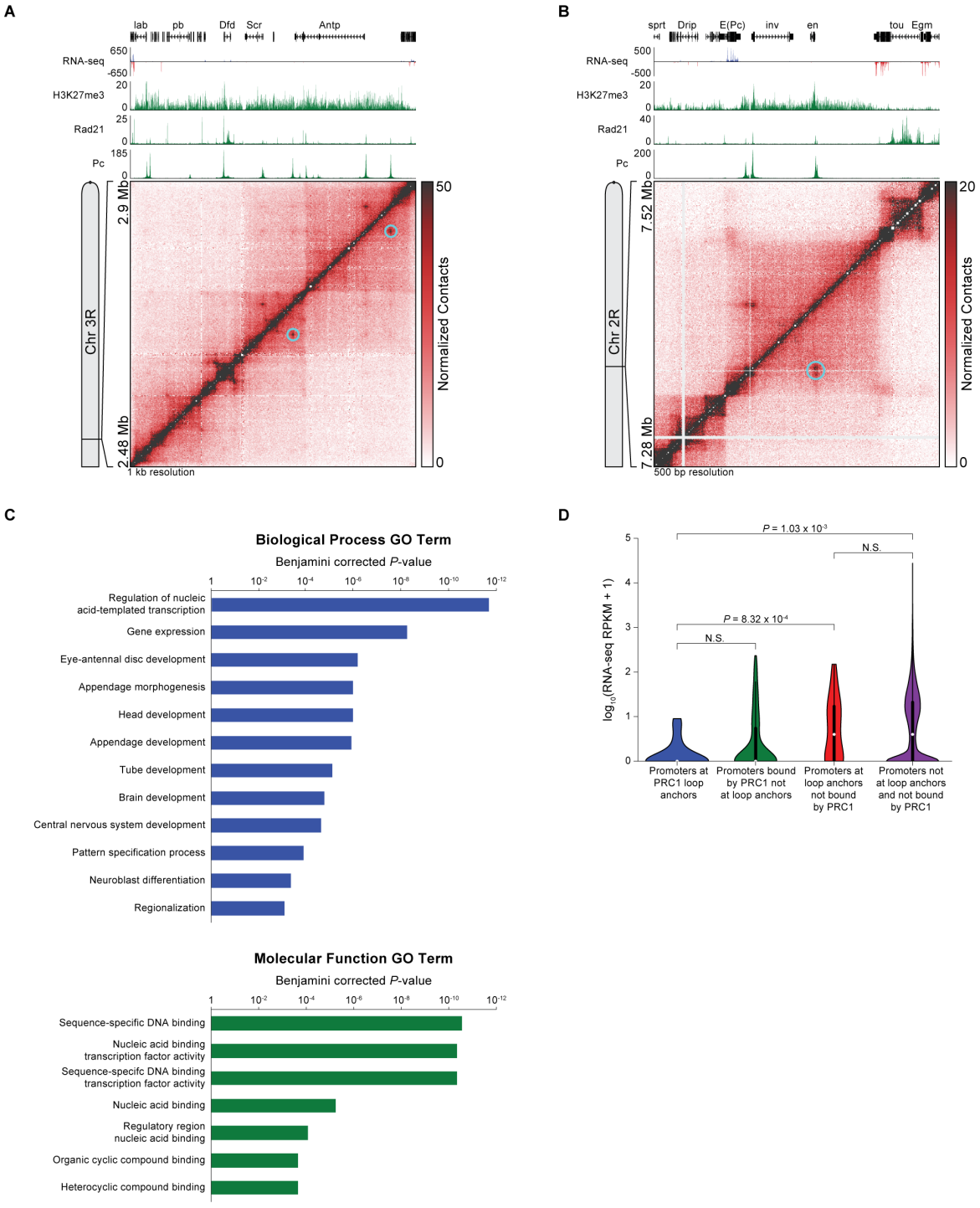

Fig. 3. Developmentally regulated promoters are found at PRC1 loop anchors.

725 **(A)** Hi-C contact map at 1 kb resolution shows chromatin loops (cyan circles) at the
726 ANT-C Hox gene complex. RNA-seq, histone H3K27me3, Rad21, and *Pc* ChIP-Seq
727 profiles are aligned above the map.
728 **(B)** Hi-C contact map at 500 bp resolution shows chromatin loops (cyan circles) at the
729 *inv* and *en* promoters. RNA-seq, histone H3K27me3, Rad21, and *Pc* ChIP-Seq profiles
730 are aligned above the map.
731 **(C)** GO term *P*-value chart indicates that PRC1 loop-anchor promoters are enriched for
732 genes that regulate transcription and development.
733 **(D)** Promoters a PRC1 loop anchors are less likely to be expressed than promoters at
734 loop anchors not bound by PRC1 (P = 8.34 x 10^{-4}; one-sided Mann–Whitney *U*-test) or
735 promoters not at loop anchors and not bound by PRC1 (P = 1.03 x 10^{-3}; one-sided
736 Mann–Whitney *U*-test). Expression levels indicated by violin plots that are overlaid with
737 Tukey box plots (black) and the median expression level (white circle). N.S., not
738 significant.
739

Figure S1

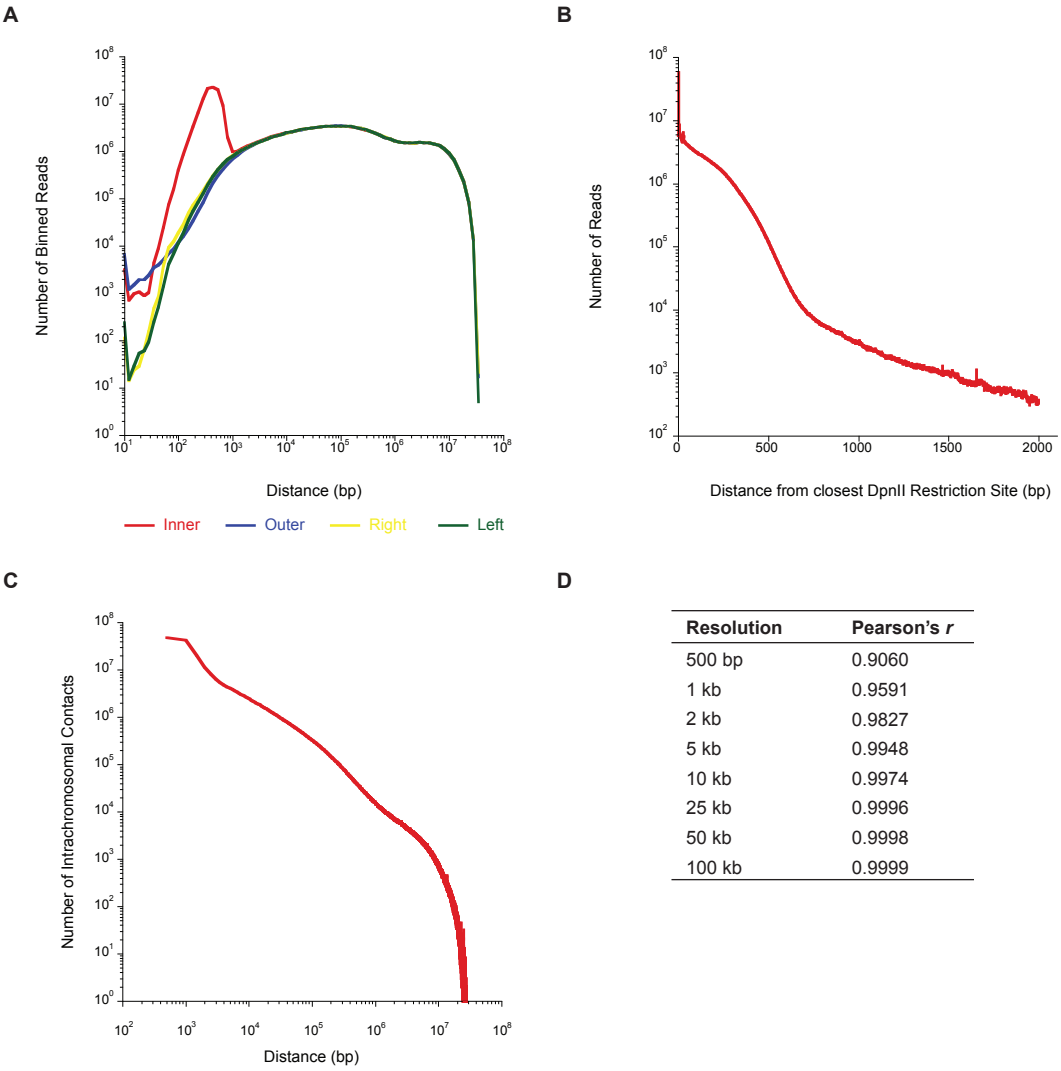

D

Resolution	Pearson's *r*
500 bp	0.9060
1 kb	0.9591
2 kb	0.9827
5 kb	0.9948
10 kb	0.9974
25 kb	0.9996
50 kb	0.9998
100 kb	0.9999

Fig. S1. Quality assessment and reproducibility of sub-kilobase resolution *Drosophila* Hi-C.

(A) Distribution of four read orientations (inner, outer, left, right) as a function of distance between reads.

(B) Number of reads at the distance indicated on the abscissa to the closest DpnII site.

(C) Number of intrachromosomal contacts separated by the distance given on the abscissa.

748 **(D)** Pearson's *r* between biological replicates at the indicated Hi-C contact map

749 resolution. Replicates were highly correlated at all resolutions.

750

Figure S2

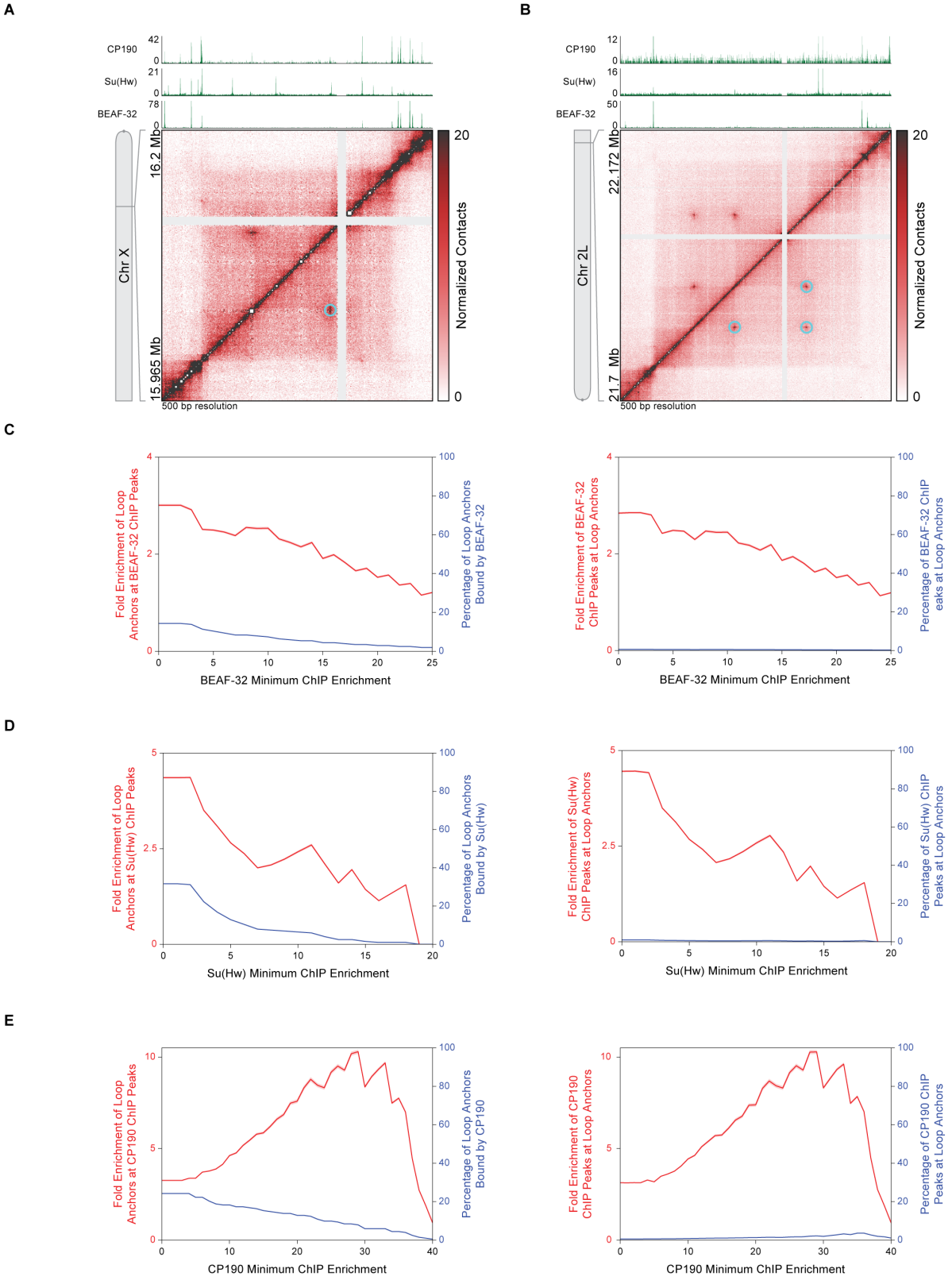

751

752 **Fig. S2. *Drosophila* insulators BEAF-32, Su(Hw), and CP190 are not strongly**
753 **enriched at loop anchors.**

754 **(A)** Hi-C contact map at 500 bp resolution reproduced from Fig. 2A of a region of
755 chromosome X shows chromatin loops (cyan circles). CP190, Su(Hw), and BEAF-32
756 ChIP-seq profiles are aligned above the map.

757 **(B)** Hi-C contact map at 500 bp resolution reproduced from Fig. 2B of a region of
758 chromosome 2L shows a small network of chromatin loops (cyan circles). CP190,
759 Su(Hw), and BEAF-32 ChIP-seq profiles are aligned above the map.

760 **(C)** Left, fold enrichment of loop anchors at BEAF-32 ChIP peaks (red) and percentage
761 of loop anchors bound by BEAF-32 (blue) at the BEAF-32 minimum ChIP enrichment
762 indicated on the abscissa. Right, fold enrichment of BEAF-32 ChIP peaks at loop
763 anchors (red) and percentage of BEAF-32 ChIP peaks at loop anchors (blue) at the
764 BEAF-32 minimum ChIP enrichment indicated on the abscissa. Red shading indicates
765 95% confidence interval.

766 **(D)** Same as **(C)** except for Su(Hw).

767 **(E)** Same as **(C)** except for CP190.

768

Figure S3

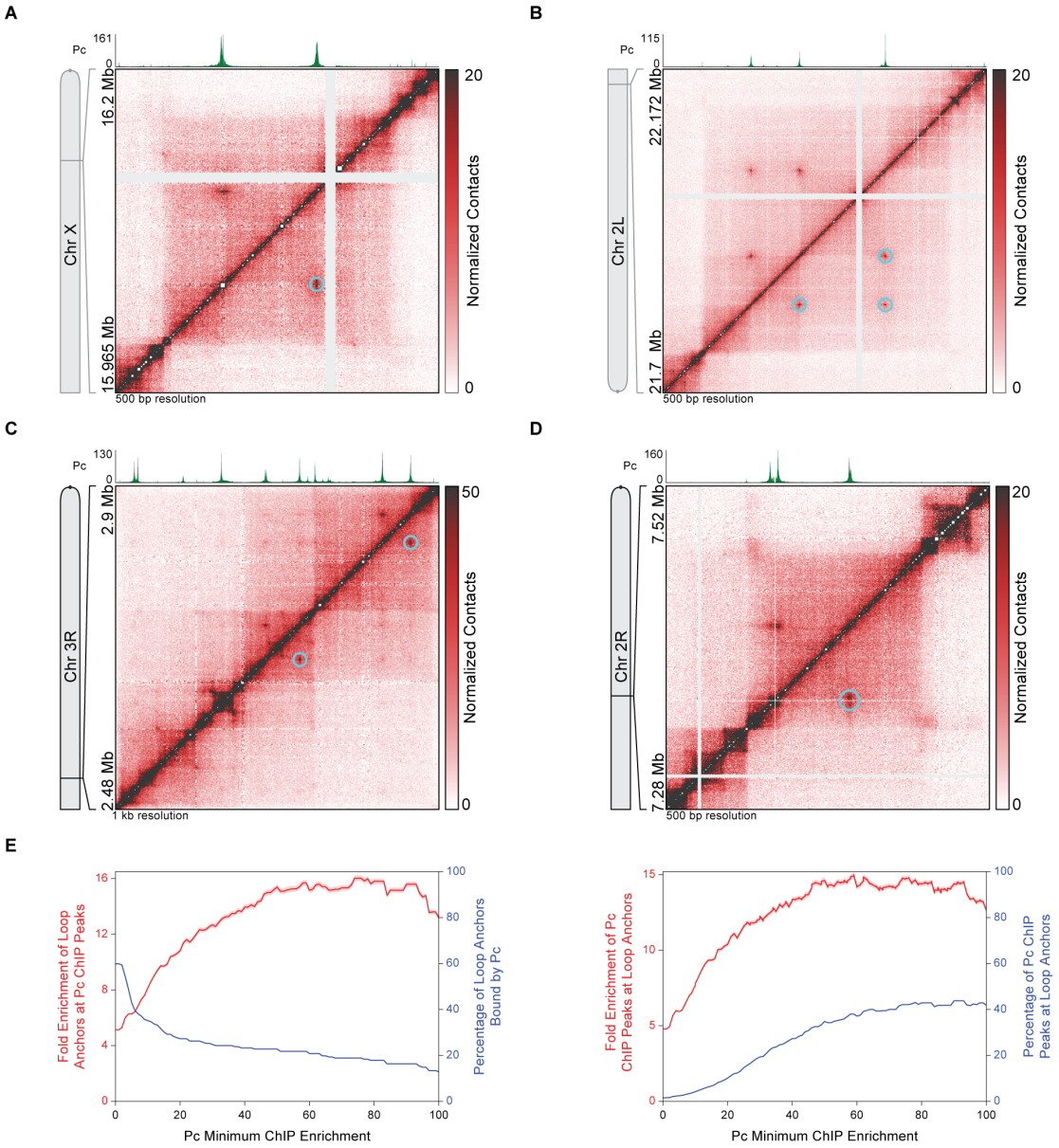

Fig. S3. Validation of PRC1 subunit Pc at Loop Anchors.

(A) Hi-C contact map at 500 bp resolution reproduced from Fig. 2A of a region of chromosome X shows chromatin loops (cyan circles) that align with Pc ChIP-seq peaks. Pc ChIP-seq profile from an antibody different from that in Fig. 2A is aligned above the map.

775 **(B)** Hi-C contact map at 500 bp resolution reproduced from Fig. 2B of a region of
776 chromosome 2L shows a small network of chromatin loops (cyan circles) that align with
777 Pc ChIP-seq peaks. Pc ChIP-seq profile from an antibody different from that in Fig. 2B
778 is aligned above the map.
779 **(C)** Hi-C contact map at 1 kb resolution reproduced from Fig. 3A shows chromatin loops
780 (cyan circles) at the ANT-C Hox gene complex that align with Pc ChIP-seq peaks. Pc
781 ChIP-seq profile from an antibody different from that in Fig. 3A is aligned above the
782 map.
783 **(D)** Hi-C contact map at 500 bp resolution reproduced from Fig. 3B shows chromatin
784 loops (cyan circles) at the *inv* and *en* promoters that align with Pc ChIP-seq peaks. Pc
785 ChIP-seq profile from an antibody different from that in Fig. 3B is aligned above the
786 map.
787 **(E)** Left, fold enrichment of loop anchors at Pc ChIP peaks (red) and percentage of loop
788 anchors bound by Pc (blue) at the Pc minimum ChIP enrichment indicated on the
789 abscissa. Right, fold enrichment of Pc ChIP peaks at loop anchors (red) and
790 percentage of Pc ChIP peaks at loop anchors (blue) at the Pc minimum ChIP
791 enrichment indicated on the abscissa. Pc ChIP peaks are from ChIP-seq data from an
792 antibody different from that in Fig. 2F. Red shading indicates 95% confidence interval.
793

Figure S4

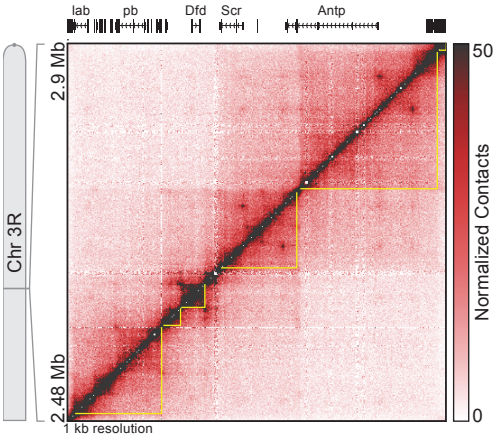

794

795 **Fig. S4. TAD organization at the ANT-C Hox gene complex.**

796 Hi-C contact map at 1 kb resolution reproduced from Fig. 3A shows that each TAD

797 (yellow outlines) at the ANT-C Hox gene complex contains one, or, at most, two

798 homeotic gene promoters.

799

Figure S5

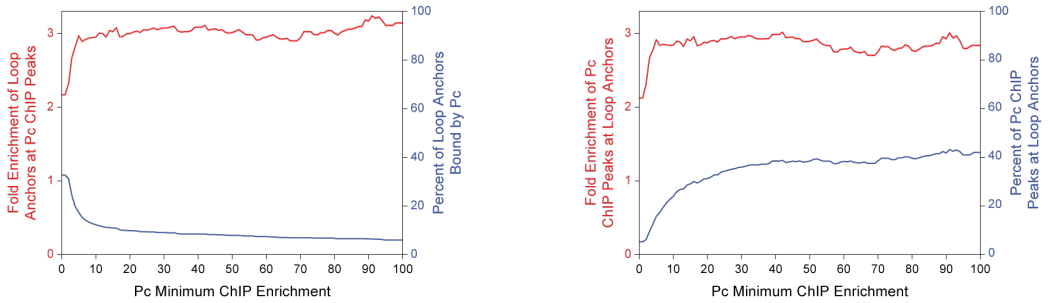

Fig. S5. Enrichment of PRC1 subunit Pc at an Independent Set of Loop Anchors. Left, fold enrichment of loop anchors at Pc ChIP peaks (red) and percentage of loop anchors bound by Pc (blue) at the Pc minimum ChIP enrichment indicated on the abscissa. Right, fold enrichment of Pc ChIP peaks at loop anchors (red) and percentage of Pc ChIP peaks at loop anchors (blue) at the Pc minimum ChIP enrichment indicated on the abscissa. Loop anchors are from reference 26 and were converted from the dm6 to dm3 genome assembly using the FlyBase *Drosophila* Sequence Coordinates Converter. Red shading indicates 95% confidence interval.

Figure S6

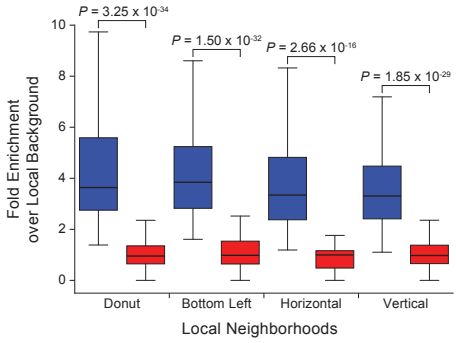

Fig. S6. Enrichment of Hi-C Contacts at Loops.

Box plots of the number of Hi-C contacts at manually annotated loops compared to the number of Hi-C contacts in four local neighborhoods (donut, bottom left, horizontal, vertical; see reference (3) for full definitions). Enrichment at manually annotated loops was significantly greater than the enrichment at a control set of randomly shuffled loops. Significance computed using a one-sided Mann–Whitney *U*-test.

Figure S7

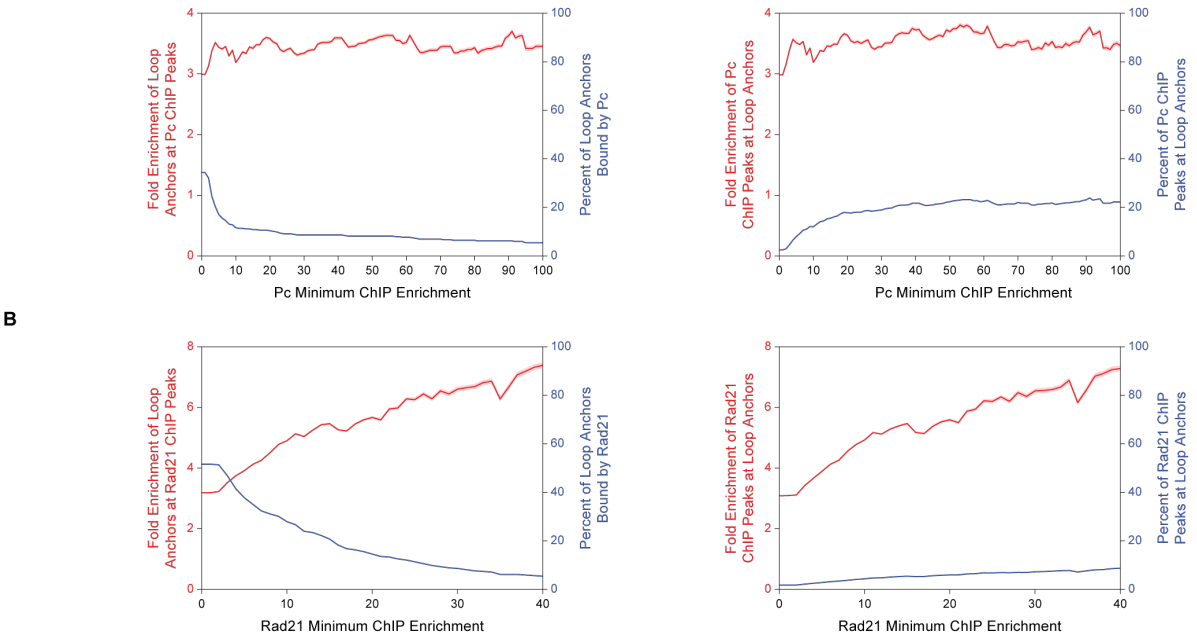

Fig. S7. Enrichment of Pc and Rad21 at HiCCUPS-Annotated Loop Anchors.

(A) Left, fold enrichment of loop anchors at Pc ChIP peaks (red) and percentage of loop anchors bound by Pc (blue) at the Pc minimum ChIP enrichment indicated on the abscissa. Right, fold enrichment of Pc ChIP peaks at loop anchors (red) and percentage of Pc ChIP peaks at loop anchors (blue) at the Pc minimum ChIP enrichment indicated on the abscissa. Loop anchors are from loops identified by HiCCUPS (see *SI Appendix, Supplementary Materials and Methods*). Red shading indicates 95% confidence interval.

(B) Same as **(A)** except for Rad21.

829 **Table S1. Hi-C sequencing statistics and quality metrics.**

	Primary	Replicate	Merged
Sequencing Statistics			
Sequenced Reads	532,673,670	554,361,974	1,087,035,644
Alignment Statistics*			
Normal Paired	395,699,521 (74.29%)	408,451,484 (73.68%)	804,151,005 (73.98%
Chimeric Paired	87,524,998 (16.43%)	92,918,735 (16.76%)	180,443,733 (16.60%)
Unmapped	10,388,903 (1.95%)	10,203,756 (1.84%)	20,592,659 (1.89%)
Ligation Motif Present	247,207,877 (46.41%)	264,925,937 (47.79%)	512,133,814 (47.11%)
Complexity Statistics*			
Alignable (Normal+Chimeric)	483,224,519 (90.72%)	501,370,219 (90.44%)	984,594,738 (90.58%)
Unique Reads	408,175,481 (76.63%)	424,129,873 (76.51%)	832,305,354 (76.57%)
PCR Duplicates	74,802,581 (14.04%)	77,032,979 (13.90%)	151,835,560 (13.97%)
Optical Duplicates	246,457 (0.05%)	207,367 (0.04%)	453,824 (0.04%)
Unique Read Statistics**			
Intra-fragment Reads	25,145,283 (4.72% / 6.16%)	25,523,374 (4.60% / 6.02%)	50,668,657 (4.66% / 6.09%)
Below MAPQ30	123,173,623 (23.12% / 30.18%)	129,753,530 (23.41% / 30.59%)	252,927,153 (23.27% / 30.39%)
Hi-C Read Statistics**			
Hi-C Contacts	259,856,575 (48.78% / 63.66%)	268,852,969 (48.50% / 63.39%)	528,709,544 (48.64% / 63.52%)
Ligation Motif Present	95,704,474 (17.97% / 23.45%)	101,798,673 (18.36% / 24.00%)	197,503,147 (18.17% / 23.73%)
3' Bias (Long Range)	69% - 31%	70% - 30%	70% - 30%
Pair Type % (L-I-O-R)	25% - 25% - 25% - 25%	25% - 25% - 25% - 25%	25% - 25% - 25% - 25%
Inter-chromosomal	12,056,707 (2.26% / 2.95%)	12,038,653 (2.17% / 2.84%)	24,095,360 (2.22% / 2.90%)
Intra-chromosomal	247,799,868 (46.52% / 60.71%)	256,814,316 (46.33% / 60.55%)	504,614,184 (46.42% / 60.63%)
Short Range (< 20 kb)	107,655,986 (20.21% / 26.37%)	114,484,535 (20.65% / 26.99%)	222,140,521 (20.44% / 26.69%)
Long Range (> 20 kb)	140,138,997 (26.31% / 34.33%)	142,325,315 (25.67% / 33.56%)	282,464,312 (25.98% / 33.94%)

830 * % Sequenced Reads

831 † % Sequenced Reads / % Unique Reads

832 For definitions of each metric see reference 3.

Table S2. Kc167 TAD coordinates.

Juicebox format. dm3 genome assembly.

See attached Excel file.

Table S3. Kc167 loop coordinates.

Juicebox format. dm3 genome assembly.

See attached Excel file.

Table S4. Complete GO terms for PRC1 loop anchors.

See attached Excel file.

842 **Table S5. External datasets used in this study.**

External Dataset	Reference	Accession Number	Antibody (if given/applicable)	Notes
Kc167 5 chromatin classes	12	GSE22069		
Kc167 BEAF-32 ChIP-Seq	11	GSE30740		
Kc167 CP190 ChIP-Seq	11	GSE30740		
Kc167 CTCF ChIP-Seq	11	GSE30740		
Kc167 H3K27me3 ChIP-Seq	14	GSE37444	Millipore Cat. # 07-449 Lot # JBC1924326	
Kc167 Pc ChIP-Seq	15	GSE63518	RJ	Fig. 2, 3, S5, S7
Kc167 Pc ChIP-Seq	15	GSE63518	VP	Fig. S3
Kc167 RNA-seq	37	modENCODE_4395		
Kc167 Su(Hw) ChIP-Seq	11	GSE30740		
Kc167 loops (independently annotated)	26	GSE80702		Fig. S5
GM12878 Hi-C loops	3	GSE63525		
GM12878 Hi-C TADs (contact domains)	3	GSE63525		

843